Characterization of Porous β-type Tricalcium Phosphate Ceramics Formed by Physical Foaming with Freeze-Drying

Kazuaki Hashimoto * , Hiroto Oikawa , Hirobumi Shibata

Posted Date: 3 April 2024

doi: 10.20944/preprints202404.0267.v1

Keywords: porous β-tricalcium phosphate; physical foaming method; freeze drying; cellulose nanofiber; non-ionic surfactants; hydrophilic/lipophilic balance (HLB)

Article

Characterization of Porous β-Type Tricalcium Phosphate Ceramics Formed by Physical Foaming with Freeze-Drying

Kazuaki Hashimoto *, Hiroto Oikawa and Hirobumi Shibata

Department of Applied Chemistry, Faculty of Engineering, Chiba Institute of Technology, 2-17-1 Tsudanuma, Narashino-shi, Chiba 275-0016, Japan; oikawa6et0@gmail.com (H.O.); hirobumi.shibata@p.chibakoudai.jp (H.S.)

* Correspondence: kazuaki.hashimoto@it-chiba.ac.jp

Abstract: Porous β-tricalcium phosphate ($Ca_3(PO_4)_2$; β-TCP) was prepared by freeze-drying and the effects of this process on pore shapes and sizes were investigated. Various samples were prepared by freezing β-TCP slurries above a liquid nitrogen surface at −180 °C with subsequent immersion in liquid nitrogen at −196 °C. These materials were then dried under reduced pressure in a freeze-dryer after which they were sintered by heating. Compared with conventional heat-based drying, the resulting pores were more spherical, which increased both the mechanical strength and porosity of the β-TCP. These materials had a wide range of pore sizes from 50 to 200 μm, with the mean and median values both approximately 100 μm regardless of the freeze-drying conditions. Mercury porosimetry data showed that the samples contained small, interconnected pores with sizes of up to 1.24 μm and macroscopic, interconnected pores up to 25.8 μm in size. The effects of non-ionic surfactants having different hydrophilic/lipophilic balance (HLB) values on foaming and pore size were also investigated. Materials made with surfactants having lower HLB values exhibited smaller pores and lower porosity whereas higher HLB surfactants gave higher porosity and slightly larger macropores. Even so, the pore diameter could not be readily controlled solely by adjusting the HLB value. The findings of this work indicated that high porosity (75%) and good compressive strength (>2 MPa) can both be obtained in the same porous material and that foaming agents with HLB values between 12.0 and 13.5 were optimal.

Keywords: porous β-tricalcium phosphate; physical foaming method; freeze drying; cellulose nanofiber; non-ionic surfactants; hydrophilic/lipophilic balance (HLB)

1. Introduction

A wide variety of synthetic materials, including metals, polymers, and ceramics, are currently being investigated with regard to clinical applications as bone substitutes [1–4]. Of particular interest are sintered calcium phosphates, especially hydroxyapatite ceramics ($Ca_{10}(PO_4)_6(OH)_2$; HAp) [5,6], β-tricalcium phosphate ceramics (β-$Ca_3(PO_4)_2$; β-TCP) [5,7] and biphasic calcium phosphate ceramic composites (BCP) [8–10]. This interest is primarily related to the fact that bone is largely composed of calcium phosphate apatite minerals. HAp implants are more crystalline than biological bone and so these implants exhibit greater chemical stability in vivo and tend not to degrade after implantation [11,12]. In the case that resorption does not occur in such implants, bone deformation [13] and the risk of fracture around the replacement bone may increase in the long term [11]. In contrast to HAp ceramics, β-TCP ceramic implants are bioabsorbable and easily replaced by new autogenous bone [14,15]. Because the solubility of these materials is close to that of living bone, these ceramics are also not soluble under physiological conditions (meaning a pH of 7.4 and temperature of 37 °C) [16] and instead are typically absorbed by osteoclasts. The associated mechanism is believed to involve local acidification leading to the dissolution of the sintered β-TCP [14,17]. In addition to this osteoconductive capacity, sintered β-TCP has been shown to exhibit significant osteoinductive characteristics [18]. For these reasons, sintered β-TCP is one of the most attractive bone replacement

 doi:10.20944/preprints202404.0267.v1

materials. In particular, porous β-TCP can be used as a scaffold material to promote the repair of bone tissue because it has suitable pore sizes to promote the growth of bone tissue within the porous material [19,20]. β-TCP also tends to contain macropores (100-600 μm) together with micropores (0.1-10 μm) and connections between these pores allow nutrients, blood, cells and biological tissue to enter, thereby promoting autogenous ossification. Many previous studies have demonstrated these effects [21–26].

Porous bodies can be produced with relative ease using foaming methods, in which a foaming agent is added and ambient air is entrained by mechanical agitation. In these techniques, the foam is typically stabilized by adding a surfactant based on the Gibbs-Marangoni effect, in which surfactant molecules compensate for surface tension gradients [27]. Prior research by the authors has demonstrated that porous materials prepared by foaming methods exhibit biases in pore size and pore distribution. This bias occurs due to various factors involved in the formation of bubbles, such as flow due to gravity, surface viscosity, the contribution of capillary attraction at the plateau boundary to membrane liquid drainage and gas diffusion associated with the coalescence and redistribution of bubbles [28]. An especially important factor is capillary attraction at the plateau boundary at which bubbles are adjacent to one another. The rate of flow to the plateau boundary has been shown to be correlated with the viscosity of the adsorption layer near the surface. It has also been reported that a higher viscosity will increase the thickness of the film between bubbles such that the bubble lifetime is increased [29]. The Young-Laplace equation [30] describing gas diffusion states that, in the case that two bubbles of different sizes come into contact with one another, the air from the smaller bubble (which has a higher internal pressure) will diffuse through the bubble film towards the larger bubble. As a consequence, smaller bubbles are absorbed by larger bubbles, causing the bubbles to merge and resulting in the disappearance of some bubbles.

The authors previously attempted to fabricate porous materials by adding a nonionic surfactant to β-TCP slurries as a foaming agent together with cellulose nanofibers (CNFs) as a thickening agent and bubble stabilizer. These additives were employed in conjunction with a physical foaming method in which pores were formed by mechanical stirring. This prior work showed that, in trials using a conventional foaming method, pores were uniformly distributed throughout the specimens and porous bodies with high mechanical strength of the slurry hardened body could be obtained. It was also found that the gravity-induced outflow of water into the lower layers and the coalescence of bubbles prevented the pores from concentrating at the top of the sample and prevented the pores from coarsening [31]. However, using this method, it was challenging to properly disperse the CNFs and these fibers tended to agglomerate during drying in association with heating. This agglomeration resulted in sintered porous bodies having irregular pore shapes rather than spherical pores. In later work, porous materials were generated using CNFs in which some of the -OH groups on the CNFs were acetylated [32] or replaced by phosphite groups [33]. The resulting porous materials were found to have spherical pores. Furthermore, we prepared porous β-TCP by a similar method, instead of CNFs with the thickening effect of carboxymethylcellulose ammonium salt, and found that porous β-TCP could be prepared with suitable pore size, porosity and mechanical strength for bone filling material, without any difference in pore size distribution according to the sample location [34].

In the present study, foamed β-TCP slurries were rapidly frozen and solidified, after which dried porous materials were obtained from the frozen specimens, from which water was removed by freeze-drying. This was an alternative to slower heat-based drying. The freeze-drying method used in this work was superior in that the water in the slurry was rapidly frozen at reduced pressure, after which the material was returned to room temperature such that the water evaporated without going through the liquid phase. This process allowed the samples to be dried without destroying the pore structure of the frozen slurry. The effects of varying the fabrication conditions were investigated with a focus on quick freezing. Porous specimens were also fabricated using nonionic surfactants with different hydrophilic/lipophilic balance (HLB) values [35] to control the pore size, and the physical properties of the resulting porous materials were evaluated.

 doi:10.20944/preprints202404.0267.v1

2. Experimental

2.1. Preparation of Raw Powder

In this procedure, 11.32 g of calcium carbonate ($CaCO_3$, purity 99.0%, Fujifilm Wako Pure Chemicals, Osaka, Japan) and 39.51 g of calcium hydrogen phosphate dihydrate ($CaHPO_4{\cdot}2H_2O$, purity 99.5%, Fujifilm Wako Pure Chemicals, Osaka, Japan) were mixed in a Ca/P molar ratio of 1.50. This mixture was subsequently combined with 450 ml pure water heated to 80 °C, and then ground using zirconia balls (Nikkato Corporation, Osaka, Japan; YSZ balls, 400 g) in a zirconia pot (As One Corporation, Osaka, Japan) having dimensions of 100 mm (width) × 130 mm (height) for 24 h. Each mixed sample was then spread in a plastic container and dried at 70°C for 24 h. Following this, each dried specimen was ground using an agate mortar and then calcined in an electric furnace by heating to 750 °C at 3 °C/min with a hold time of 10 h. The calcined powders were characterized by X-ray diffraction (XRD, MiniFlex 600: Rigaku Corporation, Tokyo, Japan), Fourier transform infrared (FT-IR) spectroscopy (FT-IR-4200: JASCO Corporation, Tokyo, Japan) and scanning electron microscopy (SEM, VE-7800: KEYENCE Corporation, Tokyo, Japan).

2.2. Preparation of Porous Materials by Freeze-Drying

In each trial, 30 g of the calcined powder was mixed with 30 g of a 3.0 wt% dispersion of CNFs in water (fiber width: 0.069 μm, fiber length: 9.66 μm: Daio Paper Corporation, Shikoku, Japan) together with 30 ml of ammonium polyacrylate solution 70-110 (molecular weight: approximately 10,000, Fujifilm Wako Pure Chemicals, Osaka, Japan), diluted to 5 vol% and dispersed in cold water using a hand blender (HB-502WJ: Cuisinart, Tokyo, Japan) in an ultrasonication device (As One, Tokyo, Japan) filled with ice water for 5 min. Subsequently, a 4 ml quantity of a polyoxyethylene alkyl ether nonionic surfactant (BT-7, Nikko Chemicals Corporation, Tokyo, Japan) was added as a foaming agent. Foaming was then carried out by mechanical agitation under the same conditions as used to produce the original dispersions. The resulting foam was tapped at a height of approximately 20 mm and poured into a polypropylene mold (25 mm in length × 25 mm in width × 25 mm in height). Each specimen was subsequently frozen by being suspended above the surface of liquid nitrogen in a stainless-steel dewar (at which location the ambient temperature was −180 °C), as shown in **Figure 1**. The sample was then pre-frozen by direct immersion in the liquid nitrogen (at a temperature of −196 °C) and then stored in a −40 °C freezer. Following this, each pre-frozen sample was freeze-dried using an FDU-1200 apparatus (EYELA, Tokyo, Japan) at −40 °C and 20 Pa. Each of the dried specimens was then sintered in an electric furnace by heating at a rate of 5 °C/min to 180 °C and holding at that temperature for 4 h followed by a 4 h hold at 300 °C, a 4 h hold at 400 °C and a 4 h hold at 1100 °C.

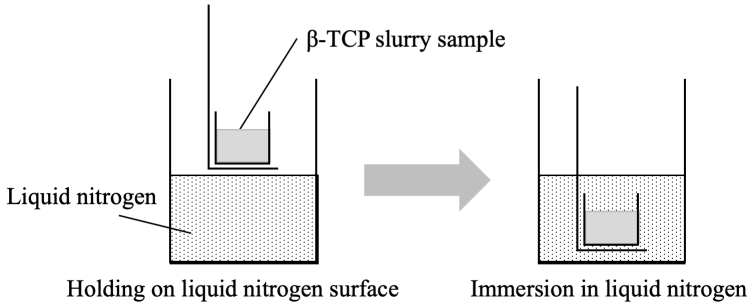

Figure 1. Schematic illustration showing pre-freezing process.

The time spans over which each specimen was held above the liquid nitrogen surface and the immersion times in the liquid nitrogen are given in **Table 1**. Note that each sample is referred to herein using the notation x-y, where x is the hold time above the liquid nitrogen [s] and y is the immersion time in the liquid nitrogen [s]. To allow a comparison of drying methods, samples were

 doi:10.20944/preprints202404.0267.v1

also prepared by heat-drying at 40 °C for 72 h using an NDO-450ND apparatus (EYELA, Tokyo, Japan) after which the same sintering program was applied.

Table 1. Hold times for samples above liquid nitrogen surface and immersion times in liquid nitrogen.

Immersion time \ Hold time	0s	10s	20s	30s	240s
0s					240-0
10s	0-10	10-10	20-10	30-10	
20s	0-20	10-20	20-20	30-20	
30s	0-30	10-30	20-30	30-30	

2.3. Preparation of Porous Materials Using Nonionic Surfactants with Different HLB Values

In these procedures, 30 ml of a 5 wt% ammonium polyacrylate solution, 30 g of a 3.0 wt% dispersion of CNFs in water and 30 g of the calcined β-TCP powder were mixed for 5 min using a hand mixer in an ultrasonication device filled with ice water. Following this, 4 ml of a polyoxyethylene alkyl ether surfactant (either BT-5, BT-7, BT-9 or BT-12, Nikko Chemicals Corporation, Tokyo, Japan) was added as a foaming agent and the specimen was foamed for 5 min. After tapping, the mixture was poured into a polypropylene mold and first frozen by holding for 30 s above the surface of liquid nitrogen then pre-frozen by direct immersion for 20 s in the liquid nitrogen. Samples were subsequently stored in a freezer. Following this, each frozen specimen was freeze-dried at −40 °C and 20 Pa. The freezing conditions were 30-20 using the notation described above. The dried samples were sintered using the method described in the previous section. The HLB values of the foaming agents used in this study were 10.5, 12.0, 13.5 and 14.5 for the BT-5, BT-7, BT-9 and BT-12, respectively [35].

2.4. Evaluation of Porous Materials

Some of the porous materials were crushed and the resulting powders were characterized by XRD and FT-IR spectroscopy. The samples were also cut into sections along the vertical direction and the pore structures of these sections were evaluated by SEM. These sections comprised the top, center and bottom parts with respect to the height direction of each sample. From the SEM images, the largest diameters of 300 randomly selected pores were determined for each specimen using the ImageJ image processing software. In addition, 30 pores were randomly selected from SEM images of the top, center and bottom sections of each specimen and the areas and perimeters of these pores were ascertained. The corresponding circularity value for each pore (having a value between 0 and 1) was then calculated as

$$\text{circularity} = 4\pi\,[\text{area}]/[\text{perimeter}]^2. \quad (1)$$

The porosity and bulk density of each material were determined by the Archimedes method following the procedure in the JIS R 1634 standard. Compressive strength tests based on the JIS R 1680 standard were carried out using a universal testing machine (Little Senstar, Tokyo Testing Machinery, Tokyo, Japan). Pore size distributions and pore volumes were obtained using the mercury injection method, employing an Autopore IV 9520 instrument (Shimadzu Corporation, Kyoto, Japan).

3. Results and Discussion

 doi:10.20944/preprints202404.0267.v1

Figure 2. presents XRD patterns obtained for sintered samples prepared with various hold and immersion times during pre-freezing. The diffraction peaks generated by all samples can be attributed to β-TCP (ICDD No. 055-0898). No peaks related to by-products such as hydroxyapatite appeared, indicating that each of the samples comprised a single β-TCP phase.

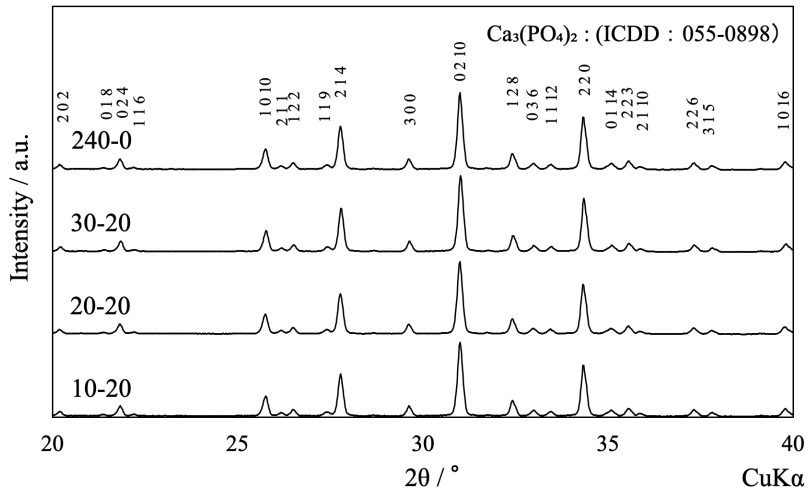

Figure 2. XRD patterns for porous samples fabricated in this work.

Figure 3 provides the FT-IR spectra of the same samples as shown in Figure 2. These spectra exhibit peaks ascribed to the bending vibration of PO_4 groups in β-TCP at 430 cm^{-1} (ν_2) and 560-600 cm^{-1} (ν_4) and the stretching vibration of PO_4 groups at 960 cm^{-1} (ν_1), 1020 cm^{-1} (ν_3) and 1120 cm^{-1} (ν_3). The absence of peaks related to the potential by-products hydroxyapatite (that is, -OH peaks) and calcium pyrophosphate (meaning P-O-P peaks) in these spectra provides further evidence that each material was pure β-TCP [36].

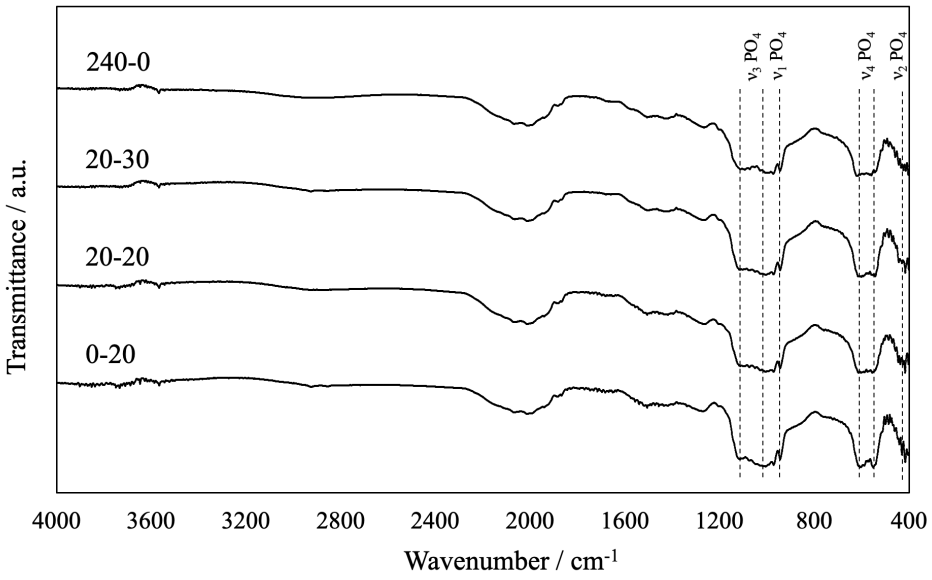

Figure 3. FT-IR spectra of porous samples fabricated in this work.

Figure 4 presents photographic images of the samples. Here, Figure 4a shows the material immersed in liquid nitrogen for 30 s and the sample is seen from above. In this case, many cracks were formed during the freezing process and it was difficult to maintain the shape of the specimen. The image in Figure 4b shows a sample immersed in liquid nitrogen but not held above the liquid nitrogen surface, as viewed from the side. Internal bubbles evidently exploded at the top of the sample and the original shape of the specimen was changed. These effects are attributed to the

 doi:10.20944/preprints202404.0267.v1

sudden temperature change caused by immersion in the liquid nitrogen. The image in Figure 4c shows a sample immersed in the liquid nitrogen for 20 s or longer with a hold time of more than 30 s above the liquid nitrogen surface, seen from the side. Compared with the specimen in Figure 4b, the shape of the sample in Figure 4c was hardly distorted, indicating that the sample morphology could be maintained by using hold and immersion times of 20 s or longer.

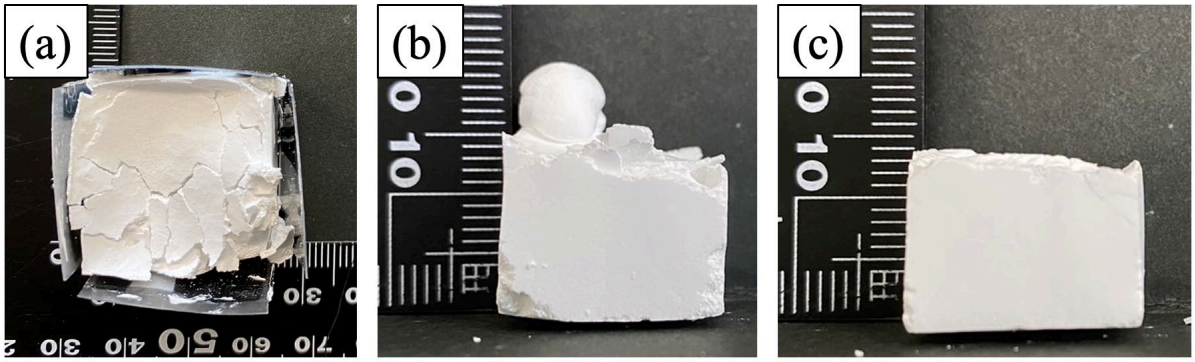

Figure 4. Photographic images of (a) 30-30 (top view), (b) 0-30 (side view) and (c) 30-20 (side view) specimens.

Figure 5 shows cross-sectional SEM images of a sample immersed in the liquid nitrogen for 10 s with no hold time above the liquid nitrogen and a sample held above the liquid nitrogen for 240 s but with no immersion. The 240-0 sample exhibits spherical pores along with many crack-like pores that distort the spherical pore shapes. Holding this sample for 240 s above the liquid nitrogen caused it to freeze more slowly due to the lower thermal conductivity of the gaseous nitrogen. This, in turn, promoted the growth of ice crystals in the sample, and the sublimation of this ice during subsequent freeze-drying is thought to have produced the crack-like pores. The SEM images of the sample immersed in the liquid nitrogen for 10 s confirm the formation of spherical pores in the top and bottom parts of the sample whereas the center part contained numerous cracks similar to those in the 240-0 specimen. These results suggest that a 10 s immersion in the liquid nitrogen was not sufficient to freeze the specimen such that subsequent cooling froze the center part.

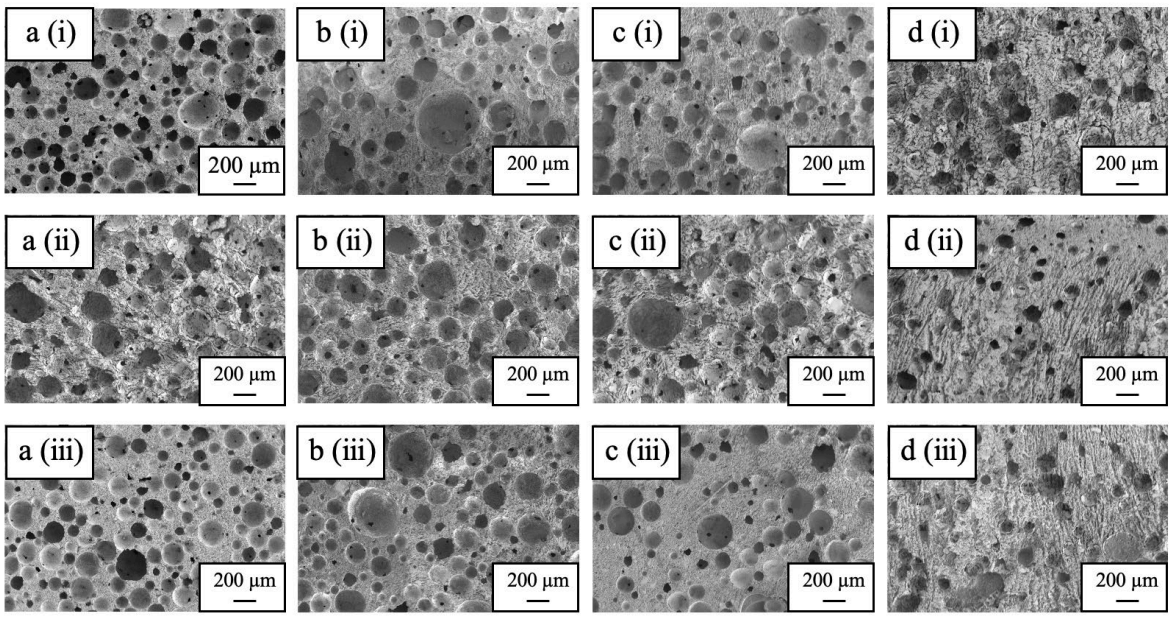

Figure 5. SEM images of cross-sections of (a) 0-10, (b) 20-10, (c) 30-10 and (d) 240-0 specimens, showing (i) top, (ii) center and (iii) bottom sections.

 doi:10.20944/preprints202404.0267.v1

Figure 6 presents cross-sectional SEM images of the sample immersed in the liquid nitrogen for 20 s and the samples produced with heat-drying. The latter material exhibits many distorted sphere-like pores with sizes of 200-300 μm, whereas the former sample shows spherical pores with sizes of 50-200 μm together with an interconnected pore structure. These findings indicate that the preparation of materials with spherical pores is possible based on pre-freezing with liquid nitrogen followed by freeze-drying. The sample immersed in liquid nitrogen for 20 s was evidently sufficiently frozen as no cracked pores were observed. Hence, ice crystals were not grown in this material as had occurred in the 240-0 sample.

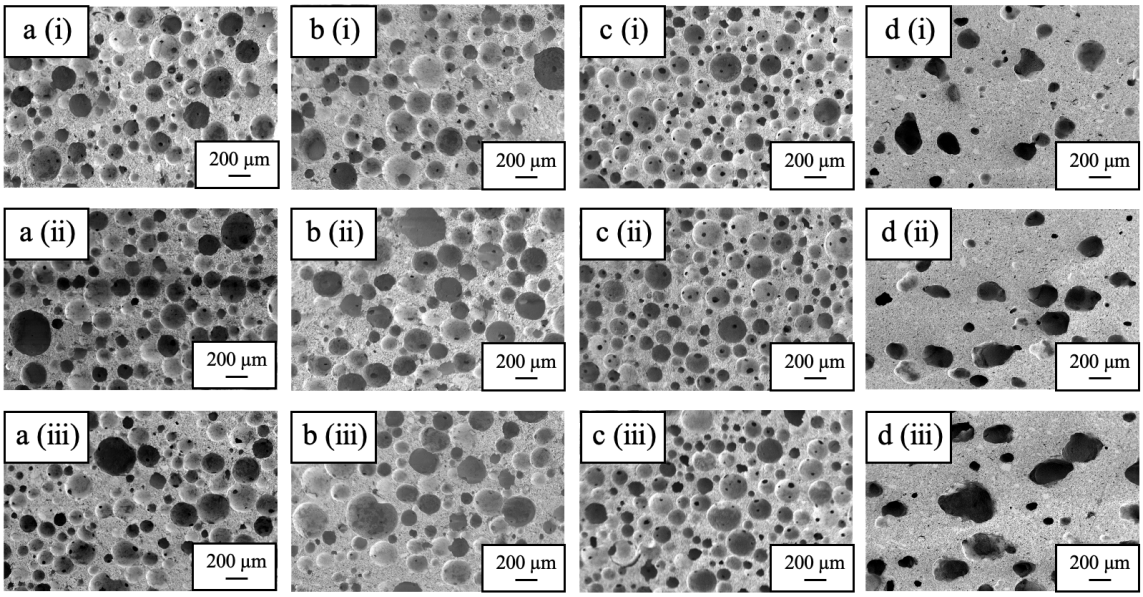

Figure 6. SEM images of cross-sections of (a) 10-20, (b) 20-20, (c) 30-20 and (d) heat-dried specimens, showing (i) top, (ii) center and (iii) bottom sections.

Table 2 summarizes the pore circularity values calculated from the SEM images of the 30-20 sample and the heat-dried material. Note that the pore circularity increases as the values approach 1.0. The values for the samples made using heat-drying differed slightly, with an average of 0.85. In contrast, the 30-20 sample produced using freeze-drying showed no difference in circularity between different sites, with an average value of 0.97. These data confirm that improved circularity was obtained relative to the heat-dried sample.

Table 2. Pore circularity values for porous β-TCP specimens obtained using different drying methods.

Location	Heat-drying (40°C, 72 h)	Freeze-drying (30-20)
Top	0.87	0.98
Center	0.82	0.97
Bottom	0.86	0.97
Average	0.85	0.97

Figure 7 provides pore diameter histograms obtained from analysis of SEM images of the 0-20, 10-20, 20-20, 30-20 and Heat-drying samples. Here, the horizontal axis represents the pore diameter

 doi:10.20944/preprints202404.0267.v1

while the vertical axis indicates the frequency. These data confirm that the pore diameters for all samples were distributed over a wide range from 50 to 200 μm. The mean and median pore sizes for the samples immersed in liquid nitrogen were all approximately 100 μm while the values for the Heat-drying sample were drastically increased. This discrepancy is attributed to the fact that cracked pores in the specimens disrupted the pore shapes and also indicates an effect whereby pores smaller than 50 μm were very difficult to observe. It is also apparent that the pore sizes for the foams did not change when the freezing conditions were changed, presumably because the foams were frozen instantaneously.

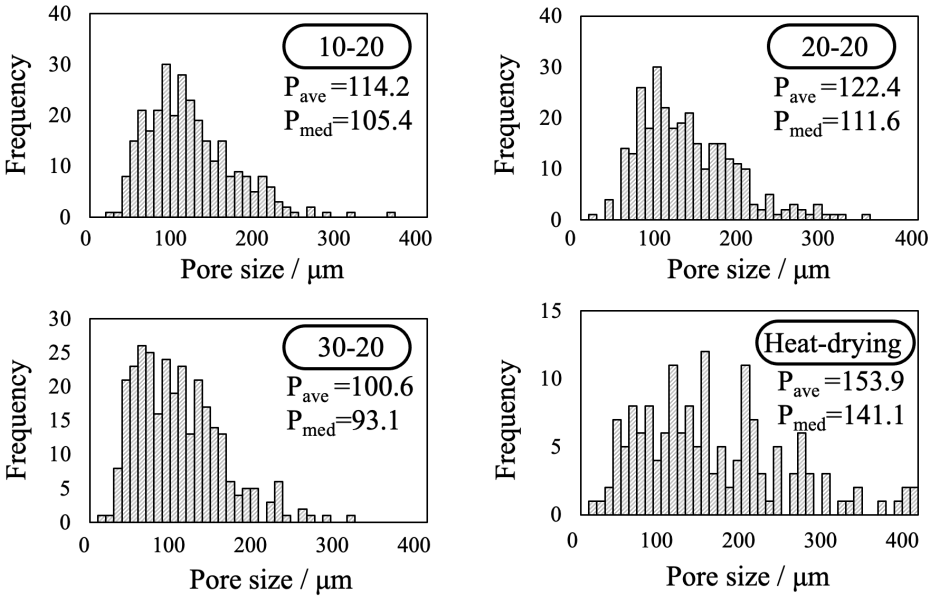

Figure 7. Pore size histograms for various porous β-TCP specimens.

The formation of pores within these materials using the different drying methods is illustrated in **Figure 8**. Drying with hot air required a longer time span such that bubbles had more time to undergo coalescence. During sintering, the CNFs were burnt off and produced pores and so the samples generated using heat-drying were more likely to have distorted sphere-like pores. In contrast, freeze-drying after instantaneous pre-freezing prevented the coalescence of bubbles, resulting in the formation of many pores with smaller diameters. The freezing of the CNFs while they were dispersed in the slurry prevented their agglomeration, providing more spherical pores [31].

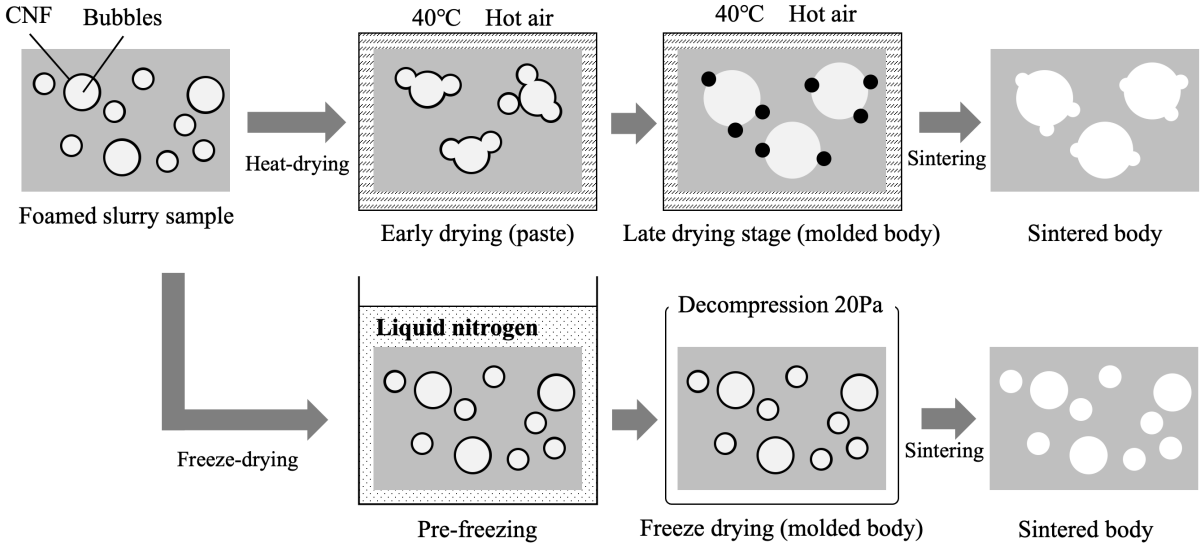

Figure 8. Schematic illustration showing pore formation in foams using different drying methods.

 doi:10.20944/preprints202404.0267.v1

Figure 9 summarizes the open porosity, closed porosity and bulk density values for each sample as ascertained using the Archimedes method. The open porosity for each of the freeze-dried specimens was approximately 70%, indicating that highly porous materials were prepared. The closed porosity values for all samples were less than 1% of the total porosities, demonstrating that these bodies should be more permeable than those prepared using heat-drying. Freeze-drying evidently increased pore connectivity because the CNFs were dispersed throughout each sample and generated pores as they were removed during sintering [31].

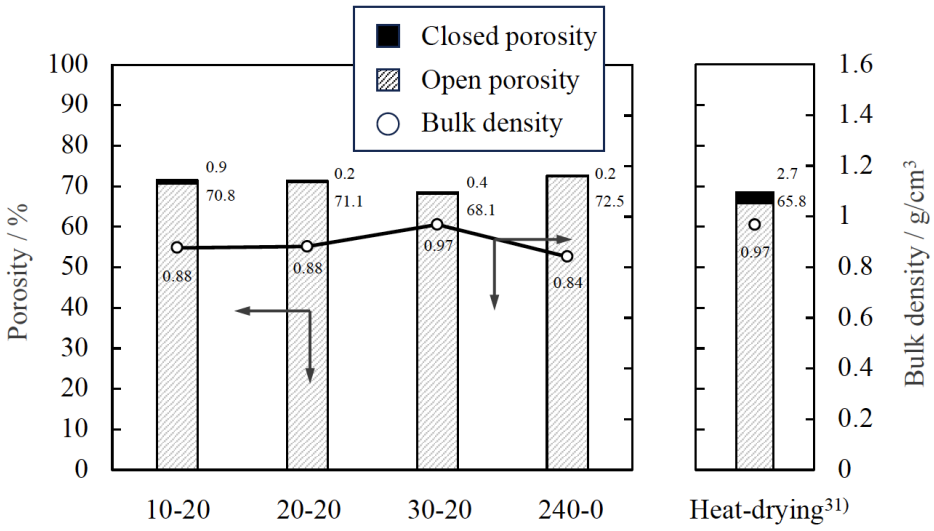

Figure 9. Bulk density and porosity values for porous β-TCP specimens as determined using Archimedes method. The directions of the arrows indicate the relationship between the axes in the figure. The numerical values for porosity indicate closed porosity in the upper part and open porosity in the lower part.

The compressive strength test results for all samples are shown in **Figure 10**. The compressive strength of each freeze-dried product exceeds 2 MPa, indicating that sufficient mechanical strength has been achieved to withstand handling. There was a correlation between the porosity of each specimen and its compressive strength, such that more porous materials had lower compressive strength. The 240-0 sample had the lowest compressive strength, which was assumed to be due to the crack-like pores observed in the SEM images. The specimens made using heat-drying had distorted sphere-like pores and therefore exhibited reduced compressive strength despite their low porosity values. Each of the materials containing only spherical pores was found to exhibit both high porosity and good compressive strength, indicating that spherical pores promoted both mechanical strength and porosity.

Preprints.org (www.preprints.org) | NOT PEER-REVIEWED | Posted: 3 April 2024 doi:10.20944/preprints202404.0267.v1

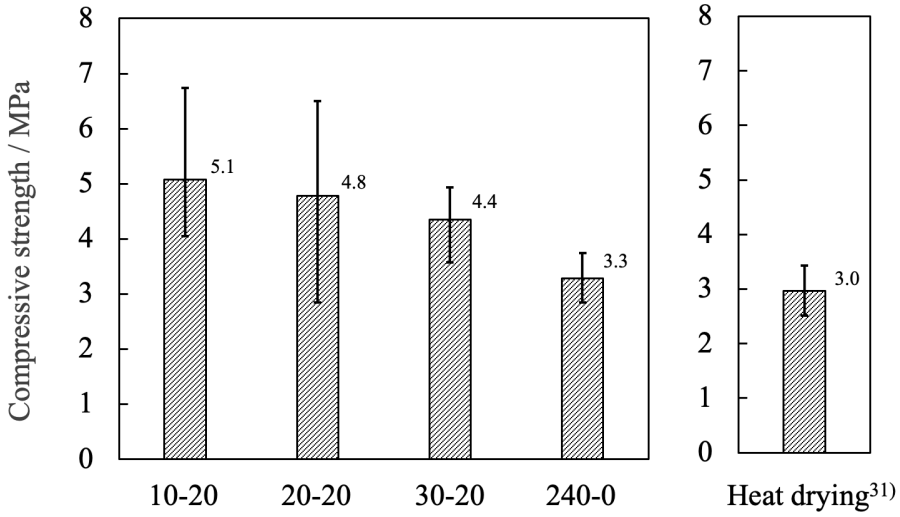

Figure 10. Compressive strength for porous β-TCP specimens fabricated in this work.

Figure 11 shows the results of pore distribution measurements by the mercury injection method for samples immersed in liquid nitrogen for 30 s, immersed for 20 s and freeze-dried or heat-dried [31]. The heat-dried sample was found to contain micropores with a maximum pore size of 0.46 μm and a wide range of macropores with sizes of 50-200 μm. The freeze-dried samples exhibited micropores with a maximum pore size of 1.24 μm and macropores with a maximum pore size of 25.8 μm in the 10-80 μm range. These data indicate a transition of the micropores to larger sizes and of the macropores to smaller sizes compared with the heat-dried samples. The micropores likely became larger due to the absence of shrinkage in the case of the freeze-dried materials, as the pore shapes changed only minimally when the specimens were dried while frozen. The macropores are thought to have shifted to smaller sizes because bubbles did not coalesce during drying. These data also suggest that the pores in these materials were connected to the exterior surfaces.

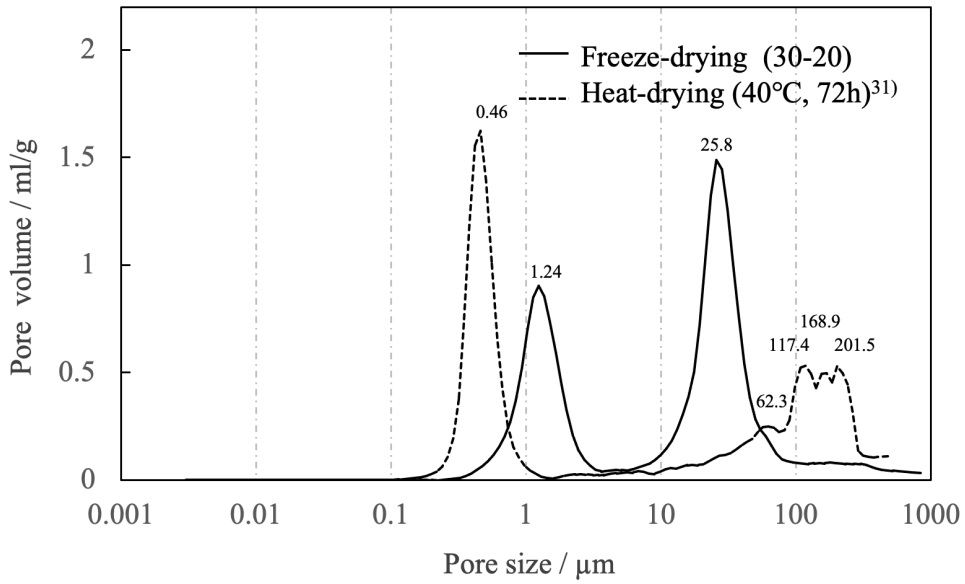

Figure 11. Pore distributions for porous β-TCP specimens fabricated by different drying methods as determined by mercury injection method.

In additional trials, the HLB value [34] for the nonionic surfactants used as foaming agents were varied. The HLB value is an indicator of the hydrophobicity/hydrophilicity of each surfactant, with a higher value reflecting a more hydrophilic compound. A nonionic surfactant having a low HLB value

 doi:10.20944/preprints202404.0267.v1

typically shows reduced foaming properties and generates smaller pores. Cross-sectional SEM images of porous β-TCP bodies prepared using nonionic surfactants with different HLB values are shown in **Figure 12**. Pores less than 50 μm in size were predominant in the sample made with the BT-5 (having an HLB of 10.5) while larger pores were obtained when using the BT-7 (HLB 12.0), BT-9 (HLB 13.5) and BT-12 (HLB 14.5). Materials with more macro-sized pores having larger pore diameters were obtained by using foaming agents with higher HLB values.

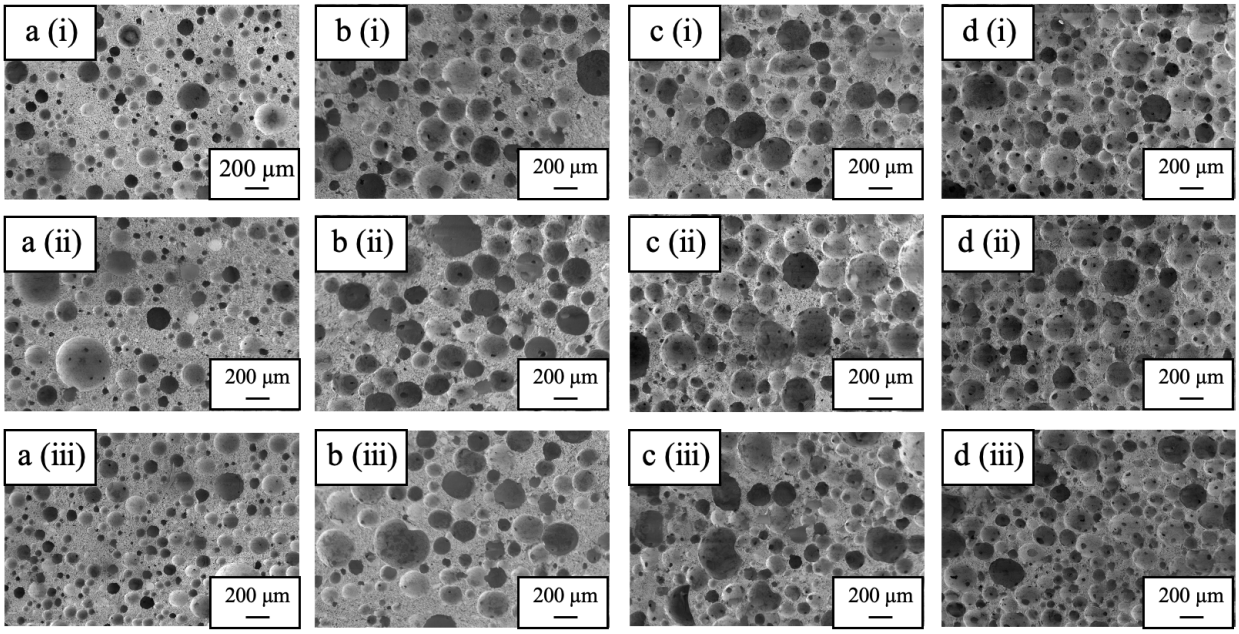

Figure 12. SEM images of cross-sections of porous β-TCP specimens fabricated using nonionic surfactants (a) BT-5, (b) BT-7, (c) BT-9 and (d) BT-12, showing (i) top, (ii) center and (iii) bottom sections.

Figure 13 provides pore size histograms for each sample as obtained by analysis of the SEM images. The average pore size and median diameter in the BT-5 sample were 88 and 73 μm, respectively, while the values obtained with the BT-7 were 100 and 93 μm, respectively, those with the BT-9 were 140 and 128 μm, respectively, those with the BT-9 were 140 and 128 μm, respectively, and those with the BT-12 were 136 and 120 μm, respectively. These results show that the addition of foaming agents with high HLB values increased both the average pore size and the median diameter. In particular, the use of the BT-9 or BT-12 came close to producing saturation and gave macro-sized pore diameters of more than 180 μm.

Preprints.org (www.preprints.org) | NOT PEER-REVIEWED | Posted: 3 April 2024 doi:10.20944/preprints202404.0267.v1

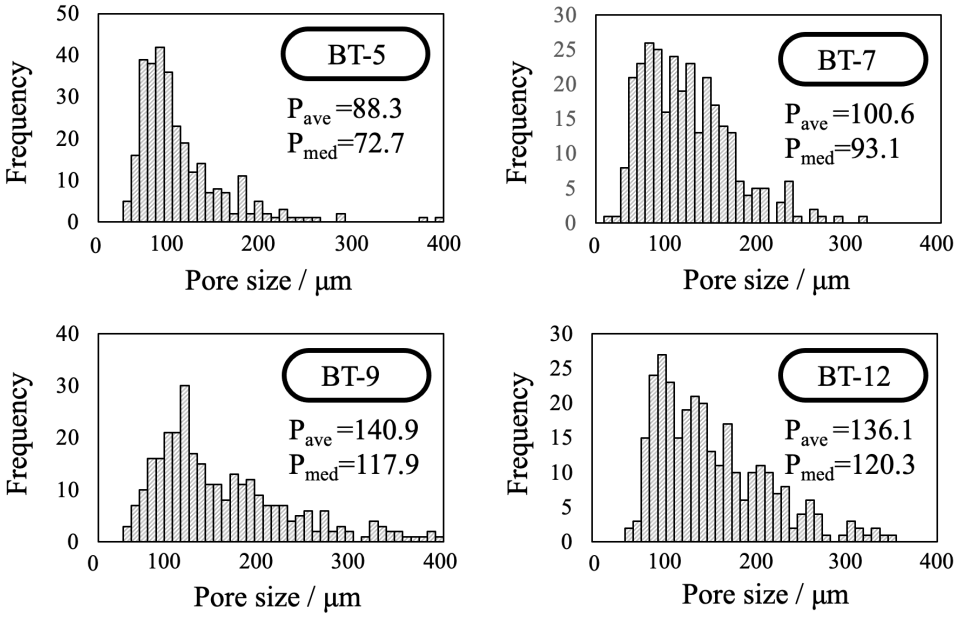

Figure 13. Pore size histograms for porous β-TCP specimens fabricated using different nonionic surfactants.

The bulk densities and porosities of the porous materials prepared by adding foaming agents with different HLB values are summarized in Figure 14. The bulk density and porosity values obtained with the BT-5 and BT-7 were approximately 0.9 g/cm³, along with open porosity values of 70%. However, the BT-9 and BT-12 provided values of approximately 0.6 g/cm³ with open porosities of 80%. In both cases, the closed porosity of the sample was almost 0%.

The compressive strengths of the various materials are provided in Figure 15. The compressive strengths of the specimens evidently decreased with the use of foaming agents having higher HLB values. The BT-9 and BT-12, both of which provided greater porosity, produced materials with strengths on the order of 1.9 MPa. Based on the above results, it appears that a foaming agent with an HLB value intermediate between those of BT-7 and BT-9 would be ideal and could produce materials simultaneously exhibiting both high porosity and good compressive strength.

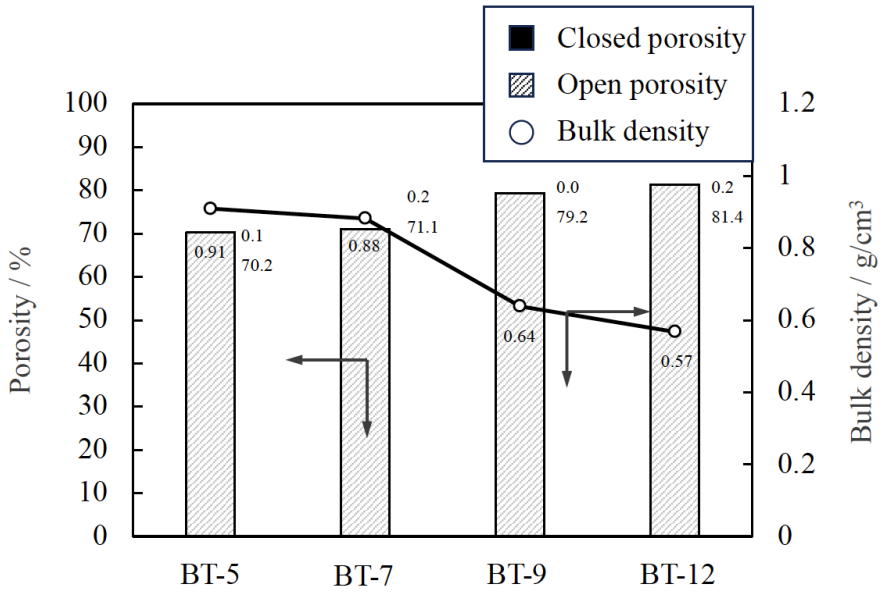

Figure 14. Bulk density and porosity values for porous β-TCP specimens fabricated using different nonionic surfactants. The directions of the arrows indicate the relationship between the axes in the

 doi:10.20944/preprints202404.0267.v1

figure. The numerical values for porosity indicate closed porosity in the upper part and open porosity in the lower part.

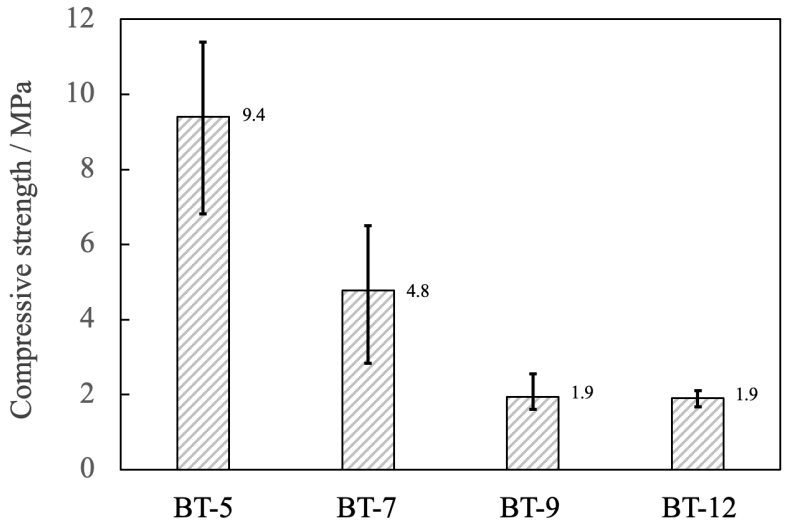

Figure 15. Compressive strength of porous β-TCP specimens fabricated using different nonionic surfactants.

4. Conclusions

The use of freeze-drying to prepare porous materials could significantly promote the formation of spherical pores to provide materials with both high compressive strength and good porosity. Such materials also exhibited exceptional permeability. Holding specimens above liquid nitrogen for several tens of seconds prior to immersion in liquid nitrogen suppressed shape changes due to ice crystal growth and a short (20 s) immersion in liquid nitrogen was found to be sufficient to freeze the samples. The specimens obtained using freeze-drying were found to be porous with a wide pore size distribution in the 50-200 μm range and had mean and median pore sizes of approximately 100 μm for all freeze-drying conditions. Mercury porosimetry results showed that the samples contained continuous micro-sized pores with a maximum pore size of 1.24 μm and continuous macro-sized pores with a maximum pore size of 10-80 μm and an average pore size of 25.8 μm. Samples made using surfactants having lower HLB values showed smaller pore diameters and reduced porosity while materials obtained using foaming agents with higher HLB values exhibited larger pore diameters with more macro-sized pores. Even so, it was not possible to control the pore size solely by adjusting the HLB value. Materials showing both high porosity (75%) and suitable compressive strength (>2 MPa) were obtained and the data suggested that the use of a foaming agent with an HLB value between 12.0 and 13.5 was optimal.

Author Contributions: K.H., H.O. and H.S. initiated the project. K.H. wrote the paper. H.O. produced all of the figures and tables. All authors participated in the discussion and interpretation of the results. All authors edited and proofread the final manuscript. All authors have read and agreed to the published version of the manuscript.

Funding: Not applicable.

Institutional Review Board Statement: Not applicable.

Informed Consent Statement: Not applicable.

Data Availability Statement: Not applicable.

Acknowledgments: The cellulose nanofibers used in this work were provided by the Daio Paper Corporation while the nonionic surfactants were obtained from the Nikko Chemicals Corporation. A part of this research was carried out in collaboration with the Daio Paper Corporation.

Conflicts of Interest: The authors declare no conflict of interest.

References

1. Kolk,A;Handschel,J;Drescher,W;Rothamel,D;Kloss,F;Blessmann,M;Heiland,M;Wolff,K.D;Smeets,R,Current trends and future perspectives of bone substitute materials – From space holders to innovative biomaterials, *J. Cranio Maxillofac.Surg*. ,2012, 40, 706-718.
2. Laurencin,C;Khan,Y; El-Amin, S.F, Bone graft substitutes, *Expert Rev. Med.*, **2006**, 3 , 49-57.
3. Giannoudis,P.V;Dinopoulos,H;Tsiridis,E, Bone substitutes: An update, *Injury* , **2005**, 36 , S20-S27.
4. Hanawa,T, Metal ion release from metal implants, *Mater. Sci. Eng. C*, **2004**, 24, 745-752.
5. Dorozhkin,S.V,Bioceramics of calcium orthophosphates, *Biomaterials*, **2010**, 31, 1465-1485.
6. Suchanek,W; Yoshimura,M, Processing and properties of hydroxyapatite-based biomaterials for use as hard tissue replacement implant, *J.Mater.Res.*, **1998,** 13 , 94-117.
7. Bohner,M;Santoni,B.L.G;Döbelin,N, β-tricalcium phosphate for bone substitution: Synthesis and properties, *Acta Biomater.*, **2020**, 113, 23-41.
8. Owen,G.Rh;Dard,M.;Larjava,H, Hydoxyapatite/beta-tricalcium phosphate biphasic ceramics asregenerative material for the repair of complex bone defects, *J.Biomed.Mater.Res. Part B Appl. Biomater.*, **2018**, 106, 2493-2512.
9. Legeros,R.Z;Lin,S;Rohanizadeh,R;Mijares,D;Legeros,J.P,Biphasic calcium phosphate bioceramics: preparation, properties and applications, *J. Mater. Sci. Mater. Med*., **2003**, 14, 201-209.
10. Bouler,J.M;Pilet,P;Gauthier,O;Verron,E, Biphasic calcium phosphate ceramics for bone reconstruction: A review of biological response, *Acta Biomater*., **2017**, 53, 1-12.
11. Linhart,W;Briem,D;Amling,M;Rueger,J.M;Windolf,J,Mechanical failure of porous hydroxyapatite ceramics 7.5 years after implantation in the proximal tibial, *Unfallchirurg* ,**2004**, 107,154-157.
12. Ogose,A;Hotta,T;Kawashima,H;Kondo,N;Gu,W;Kamura,T;Endo,N, Comparison of hydroxyapatite and beta tricalcium phosphate as bone substitutes after excision of bone tumors**,** *J.Biomed.Mater. Res.Part B Appl. Biomater.* **, 2005,** 72 ,94-101.
13. Shimazaki,K; Mooney,V, Comparative study of porous hydroxyapatite and tricalcium phosphate as bone substitute, *J. Orthop. Res.* , **1985**, 3, 301-310.
14. Eggli,P.S;Muller,W;Schenk,R.K,Porous Hydroxyapatite and Tricalcium Phosphate Cylinders with Two Different Pore Size Ranges Implanted in the Cancellous Bone of Rabbits: A Comparative Histomorphometric and Histologic Study of Bony Ingrowth and Implant Substitution *Clin. Orthop. Relat. Res.*, ***1988***, (232) 127-138.
15. Bohner,M;Baroud,G;Bernstein,A;Döbelin,N;Galea,L;Hesse,B;Heuberger,R;Meille,S;Michel,P;Rechenberg, B. von; Sague,J;Seeherman,H, Characterization and distribution of mechanically competent mineralized tissue in micropores of β-tricalcium phosphate bone substitutes, *Mater. Today*, **2017**, 20, 106-115.
16. Bohner,M;Lemaitre,J; Can bioactivity be tested in vitro with SBF solution?, *Biomaterials*, **2009**, 30 ,2175-2179.
17. Kondo,N;Ogose,A;Tokunaga,K;Ito,T;Arai,K;Kudo,N;Inoue,H;Irie,H;Endo,N, Bone formation and resorption of highly purified β-tricalcium phosphate in the rat femoral condyle, *Biomaterials* , **2005**，26, 5600-5608.
18. H.Yuan,H.Fernandes,P.Habibovic,J.de Boer,A.M.Barradas,A.de Ruiter, W.R.Walsh,C.A.van Blitterswijk,J.D.de Bruijn, Osteoinductive ceramics as a synthetic alternative to autologous bone grafting, *Proc. Natl. Acad. Sci. U.S.A.* **2010**, 107**,** 13614-13619.
19. Özgür Engin, N; Cüneyt Taş ,A; Preparation of Porous $Ca_{10}(PO_4)_6(OH)_2$ and β-$Ca_3(PO_4)_2$ Bioceramics, *J. Am. Ceram. Soc.*,**2000**, 83**,**1581-1584.
20. Bohner,M;Baumgart,F; Theoretical model to determine the effects of geometrical factors on the resorption of calcium phosphate bone substitutes, *Biomaterials*, **2004**, 25 ,3569 -3582.
21. Dong,J;Uemura,T;Shirasaki,Y;Tateishi,T, Promotion of bone formation using highly pure porous β-TCP combined with bone marrow-derived osteoprogenitor cells, *Biomaterials*, **2002**,23, 4493-4502.
22. Levengood,S.K.L;Polak,S.J;Wheeler,M.B;Maki,A.J;Clark,S.G;Jamison,R.D;Johnson,A.J.W,Multiscale osteointegration as a new paradigm for the design of calcium phosphate scaffolds for bone regeneration, *Biomaterials*, **2010**, 31, 3552-3563.
23. Wang,X;Lin,M;Kang,Y,Engineering Porous β-Tricalcium Phosphate (β-TCP) Scaffolds with Multiple Channels to Promote Cell Migration, Proliferation, and Angiogenesis，*ACS Applied Materials & Interfaces* ,**2019,** *11* (9), 9223-9232.
24. Park,M;Lee, G;Ryu,K;Lim,W,Improvement of Bone Formation in Rats with Calvarial Defects by Modulating the Pore Size of Tricalcium Phosphate Scaffolds, *Biotechnol Bioproc.*, **2019**, *E* 24, 885–892.
25. Smoak,M;Hogan,K;Kriegh,L;Chen,C;Terrell,L.B;Qureshi,A.T;Monroe,W.T;Gimble,J.M;Hayes,D.J, Modulation of mesenchymal stem cell behavior by nano- and micro-sized β-tricalcium phosphate particles in suspension and composite structutes, *J. Nanopart. Res.*, **2015**, 17, 182.
26. Gauthier,O;Bouler,J.-M;Aguado,E;Pilet,P;Daculsi,G, Macroporous biphasic calcium phosphate ceramics:influence of macropore diameter and macroporosity percentage on bone ingrowth, *Biomaterials*, **1998**,19,133-139.

 doi:10.20944/preprints202404.0267.v1

27. Firouzi, M;Nguyen,A.V, The Gibbs-Marangoni stress and nonDLVO forces are equally important for modeling bubble coalescence in salt solutions, *Colloids and Surface A: Physicochemical and Engineering Aspects* ,**2017**, 515 , 62-68.
28. Wang, H;Wei,X;Du,Y;Wang,D, Effect of water-soluble polymers on the performance of dust-suppression foams: Wettability, surface viscosity and stability, *Colloids and Surface A: Physicochemical and Engineering Aspects*, **2019**,568, 92 -98.
29. Clint, J.H,"Surfactant Aggregation" Chapter. 11, Blackie & Son, New York (1992), 250-276.
30. Vafaei, S;Wen,D,Modification of the Young–Laplace equation and prediction of bubble interface in the presence of nanoparticles, *Advances in Colloid and Interface Science*, **2015**, 225, 1-15.
31. Sasaki,H;Shibata,H;Hashimoto,K, Fabrication of Porous β-Tricalcium Phosphate Using Cellulose-Nano-Fiber, *J. Soc. Inorg. Mater. Japan*, **2020**, 27, 155-162. in Japanese
32. Mochida,R;Shibata,H;Hashimoto,K, Preparation and Evaluation of Porous β-Type Tricalcium Phosphate by Physical Foaming Method Using Acetylated Cellulose Nanofibers, *J. Soc. Inorg. Mater., Japan*, **2022**, 29, 250-257. in Japanese
33. Toyota,G; Shibata,H; Hashimoto,K, Preparation of porous β-tricalcium phosphate by foaming method using cellulose nanofiber with different manufacturing methods as foam stabilizer, *Phosphorus Res.Bull.*, **2022**, 38, 32-36.
34. Hashimoto,K;Oikawa,H; Shibata,H; Characterization of Porous β-Tricalcium Phosphate Fabricated by Physical Foaming with a Nonionic Surfactant: Effect of Adding a Thicken, *J. Ceram. Soc. Jpn*, **2024**, 132 (in Press).
35. Griffin,W.C,Calculation of HLB Values of Non-Ionic Surfactants, *J. Soc. Cosmetic Chemists*, **1954**, 5 (4),249-256.
36. Gibson,I.R;Rehman,I; Best, S.M; Bonfield,W, Characterization of the transformation from calcium-deficient apatite to β-tricalcium phosphate. *J. Mater. Sci.: Mater. in Med.* , **2000**, 11, 533–539.